Microscopic structure and thermodynamics of a core-softened model fluid: Insights from grand canonical Monte Carlo simulations and integral equations theory

Orest Pizio,[1,a)] Hector Dominguez,[2] Yurko Duda,[3,b)] and Stefan Sokołowski[4]
[1]*Universidad Autonoma Metropolitana, Iztapalapa, 09340 Mexico, Distrito Federal, Mexico*
[2]*Instituto de Investigaciones en Materiales, UNAM, Coyoacan, 04510 Mexico, Distrito Federal, Mexico*
[3]*Programa de Ingenieria Molecular, Instituto Mexicano de Petroleo, 07730 Mexico, Distrito Federal, Mexico*
[4]*Department for the Modelling of Physico-Chemical Processes, Maria Curie-Skłodowska University, Lublin 20031, Poland*

(Received 23 November 2008; accepted 8 April 2009; published online 1 May 2009)

We have studied the microscopic structure and thermodynamic properties of isotropic three-dimensional core-softened model fluid by using extensive grand canonical Monte Carlo computer simulations and Ornstein–Zernike integral equations with hypernetted chain and Rogers–Young closures. Applied simulation tools permit to obtain insights into the properties of the model in addition to available molecular dynamics data of other authors. We discuss equation of state in the density–chemical potential projection and explore the temperature dependence of the chemical potential along different isochores. The limits of the region of anomalous behavior of the structural and thermodynamic properties are established by investigating derivatives resulting from the equation of state, pair contribution to excess entropy, and translational order parameter. Besides, we evaluate the dependence of the heat capacity on temperature and density. The microscopic structure is discussed in terms of the pair distribution functions and corresponding structure factors. We have established that the hypernetted chain approximation is not successful to capture the region of anomalies in contrast to Rogers–Young approximation, but is very accurate for high fluid densities. Thus we have studied the onset for crystallization transition within this theoretical framework. Moreover, using the replicated Ornstein–Zernike integral equations with hypernetted chain closure, we explore the possibility of glass transition and described it in terms of transition density and chemical potential. © *2009 American Institute of Physics*. [DOI: 10.1063/1.3125930]

I. INTRODUCTION

The microscopic description of the properties of water and aqueous solutions is far from being completed in spite of much effort during past decades. Several peculiarities denominated as anomalies of the structural, thermodynamic, and dynamic properties of water have been reported in literature, see, e.g., Refs. 1–5. In particular, the density, the heat capacity anomaly, and the behavior of the diffusion coefficient have been discussed together with the evolution of the microscopic structure described in terms of the pair distribution functions. It has been well documented that the diffusivity of liquid water increases with increasing pressure in a certain window of thermodynamic states. This behavior has been attributed to the competition between the local ordered tetrahedral structure of the shell of first neighbors around a given molecules and possible distortions of the structure of the first and second shell. The local ordered structure under increasing pressure changes due to the breaking of hydrogen bonds, the second neighbors possibly penetrate the first shell. Weakening of intermolecular bonding results in a higher mobility. Some other tetrahedrally bonded molecular liquids, besides water, also exhibit thermodynamic and dynamic anomalies.[5,6] In particular, the density anomaly has been observed experimentally and in simulations for a quite wide class of fluids, see, e.g., references in Ref. 7. It was argued that some anomalies for some specific fluids have relevance to the possibility of the existence of a second critical point between two liquid phases, besides common vapor-liquid critical point.[8]

Several models for intermolecular interaction potentials have been proposed to describe adequately fluid systems with anomalies. In the particular case of water, it has been shown, by using molecular dynamics simulations for the SPC-E model, that the model possesses several anomalies. In particular, the structurally anomalous region of states englobes the diffusion and density anomaly region.[3,9]

Much simpler isotropic model potentials have been developed to understand the physics behind liquid state anomalies, see, e.g., Refs. 10–14. In particular, the core-softened potentials are characterized by a repulsive core and an additional region of softer repulsion where the slope dramatically changes with respect to the core. This special region can have a form of a repulsive shoulder or a ramp. A model soft ramplike interparticle interaction with continuous potential and force has been proposed and tested in very recent

[a)]Electronic mail: pizio@servidor.unam.mx. On sabbatical leave from Instituto de Quimica de la UNAM.
[b)]Deceased February 11, 2009.

works.[10,11] These authors have used molecular dynamics simulation and integral equations theory to show that the model exhibits structural, density, and dynamic anomalies.

The principal objective of the present work is manifold. First, we would like to investigate the microscopic structure and thermodynamic properties of the fluid model with specific soft-core interaction by means of grand canonical Monte Carlo (GCMC) simulation and integral equations method, in particular, in view of its anomalous behavior in a certain region of thermodynamic states. The applied simulation method provides exact data for the pair distribution functions, internal energy, equation of state in the chemical potential–density plane and heat capacity. The GCMC data for the bulk model are of interest because they permit to localize the region of structural and thermodynamic anomalies. Besides, they serve as a benchmark to test theoretical approaches. On the other hand, computationally much less expensive integral equations yield approximate results for the above mentioned properties. We explore here the hypernetted closure and Rogers–Young (RY) approximation to the Ornstein–Zernike (OZ) equation. A detailed comparison of the results from simulation and both theoretical approaches is performed. Consequently, we evaluate accuracy of approximate theories in the entire thermodynamic region of fluid states, and specifically in the region of anomalous behavior of the system. Moreover, we can answer the question which theoretical approach is better to study the soft-core system in the ample region of density and at different temperatures. We are interested to investigate the onset for crystallization and glass transitions in high density region. Our methods intrinsically involve the notion of chemical potential, we analyze the equation of state in terms of the chemical potential, fluid density, and temperature, Thus, previous molecular dynamics studies of the dependence of pressure on temperature and density are now extended to another projection. Moreover, we pay most attention to the region of rather low temperatures, in contrast to previous studies.[10,11,15] Our results are helpful in a wider context, in particular they can be used for future studies of the present core-softened and other models exhibiting anomalies under confinement, specifically in pores and in disordered porous media. First efforts in this direction have been undertaken by us recently.[16]

II. THE MODEL AND COMPUTATIONAL METHOD

The model fluid in question consists of particles that interact via isotropic core-softened potential,[10,11]

$$u_{ff}(r) = 4\varepsilon_f[(\sigma_f/r)^{12} - (\sigma_f/r)^6] + a\varepsilon_f \exp\left[-\left(\frac{r-r_0}{\sigma_f}\right)^2\right], \tag{1}$$

where σ_f and ε_f denote the diameter and the interaction energy, respectively. These parameters serve as the length and energy units in what follows. The values of other constants in the potential are taken according to previous studies of this bulk model,[10,11] namely, $a=5$ and $r_0/\sigma_f=0.7$. Under this choice the role of attractive interactions is practically negligible, i.e., the potential has a very small attractive well.

Let us proceed to the theoretical background. As common in the theory of homogeneous fluids, we employ the method of integral equations. The OZ equation for the pair correlation function reads

$$h_{ff}(r_{12}) - c_{ff}(r_{12}) = \rho_f \int d\mathbf{r}_3 h_{ff}(r_{13}) c_{ff}(r_{32}), \tag{2}$$

where $h_{ff}(r)$ and $c_{ff}(r)$ denote the pair correlation function and the direct correlation function, respectively. The fluid density is ρ_f. The OZ equation must be supplemented by the closure relations. According to the purposes of our study we have chosen to use the hypernetted chain (HNC) closure,

$$1 + h_{ff}(r) = \exp[-\beta u_{ff}(r)]\exp[h_{ff}(r) - c_{ff}(r)], \tag{3}$$

($\beta = 1/kT$) and the RY closure,

$$1 + h_{ff}(r) = \exp[-\beta u_{ff}(r)]\left[1 + \frac{\exp[\gamma_{ff}(r)f(r)] - 1}{f(r)}\right], \tag{4}$$

where $\gamma_{ff}(r) = h_{ff}(r) - c_{ff}(r)$ and $f(r)$ is the mixing function, $f(r) = 1 - \exp(-\alpha r)$. This closure requires a choice of the value for an adjustable parameter α from the equality of pressures from the virial and compressibility routes, see, e.g., Ref. 11.

It is important to mention that the HNC closure provides the possibility to obtain the chemical potential straightforwardly from the correlation functions and to compare theoretical results with grand canonical computer simulation data. However, it has been documented that the HNC does not yield the density anomaly for the particular core-softened model in question.[10,11] Nevertheless, this closure has been used in the analysis of the structural peculiarities of the model as functions of fluid density and temperature in terms of the structural order parameter.[15]

The HNC closure does not contain any adjustable parameter and is quite simple. However, it is not thermodynamically self-consistent, i.e., the virial and compressibility routes yield, for example, different values for pressure at the same thermodynamic state. On the other hand, the RY closure is self-consistent by construction. It was shown[11] that the RY closure is qualitatively correct in describing the density anomaly. The structural properties provided by this closure have not been tested in detail with respect to computer simulation data to our best knowledge. However, this closure does not provide the chemical potential straightforwardly. Consequently, it is not feasible to extend this approximation to inhomogeneous fluids. In such studies the concept of chemical potential must be used intrinsically. We resort to grand canonical Monte Carlo method to test both closures critically. Thermodynamic results in the framework of approximations given above follow from the pair distribution function, $g_{ff}(r) = h_{ff}(r) + 1$.

We are convinced and try to show below that some modifications of applied closures are necessary in future developments to obtain better description of the structural properties of primordial importance. Then, better description of thermodynamics could be reached as well. This possibility has not been explored in the present work, however.

The grand canonical Monte Carlo simulations in this study were performed by using standard routine.[17] We simulated the systems in a cubic box of the size $L\times L\times L$ with periodic boundary conditions in all directions. The linear size of the system L/σ was taken equal to 14 at high temperatures whereas at low temperatures we have performed calculations by using larger box, $L/\sigma=20$, because the length of correlations increase with decreasing temperature. The equilibrium states were usually reached after 2×10^5 steps per atom. The averages were calculated over the next 7×10^5 steps. To avoid correlations between subsequently generated states, the sampling of averages was carried out at the intervals of 10^3 steps.

The output of simulations is given in terms of the dependence of density on the chemical potential at a given temperature. We have also calculated the heat capacity from the fluctuations of the Hamiltonian, $\mathcal{H}=U-N\mu$, where U is the potential energy of the system involving N particles. The configurational heat capacity per unit volume is then given by

$$c_v=[\langle\mathcal{H}^2\rangle-\langle\mathcal{H}\rangle^2]/(Vk_BT^2). \tag{5}$$

Besides, the pair distribution functions are obtained. We do not put emphasis on the available data for internal energy on the chemical potential in our analysis below, those will be used to explore the energy route to thermodynamics in a separate work.

On the other hand, the principal output coming from integral equations is given in terms of the distribution functions $g_{ff}(r)$. Then, the structure factor is calculated straightforwardly from the Fourier transform of the pair correlation function

$$S(q)=1+\rho_f*h_{ff}(q). \tag{6}$$

The structural order parameter is described by the pair contribution to excess entropy[15,18] (we use the same notation as in Ref. 15),

$$s_2/k_B=-2\pi\rho_f\int_0^\infty drr^2g_{ff}(r)*ln[g_{ff}(r)]-h_{ff}(r). \tag{7}$$

Moreover, the translational order parameter,[10] t,

$$t=\int|g_{ff}(x)-1|dx \tag{8}$$

is explored ($x=r\rho_f^{1/3}$).

In addition, we obtain the reduced heat capacity per particle in the HNC and RY approximations by using general expression[19]

$$\overline{c_V}=2\pi\rho_f\int drr^2g_{ff}(r)\beta u_{ff}(r)\left[\beta u_{ff}(r)-\beta\frac{\partial\omega(r)}{\partial\beta}\right], \tag{9}$$

where $\omega(r)=h_{ff}(r)-c_{ff}(r)+B_{ff}(r)$ and $B_{ff}(r)$ is the bridge function determined by the closure used ($B_{ff}(r)=\ln(1+h_{ff}(r))+\beta u_{ff}(r)-h_{ff}(r)+c_{ff}(r)$),

$$\overline{c_V}=\frac{c_v}{Nk_B}-\frac{3}{2}. \tag{10}$$

Note that the heat capacities from Eqs. (5) and (9) differ by the normalization constant (while the former is calculated per unit volume, the latter is normalized by the average number of particles). A detailed comparison of the properties coming from integral equations and computer simulations is provided below.

Finally, we define the reduced units used in this work. The reduced temperature, density and the chemical potential are defined as follows, $T_f^*=k_BT/\varepsilon_f$, $\rho_f^*=\rho_f\sigma_f^3$, and $\mu^*=\mu/\varepsilon_f$. Moreover, the reduced distance is $r^*=r/\sigma_f$ and $s_2^*=s_2/k_B$.

III. RESULTS AND DISCUSSION OF THE FLUID PHASE

We begin with a brief discussion concerning comparison of our results and those obtained previously for the model in question.[10,11,15] First, our calculations confirmed that the compressibility and virial pressures calculated from the pair distribution function following from the HNC closure do not exhibit anomalous behavior along isochores for all densities studied. However, the RY closure to the OZ equation leads to the density anomaly, as already discussed by de Oliveira *et al.*[11] In contrast to the works of de Oliveira *et al.*, our RY calculations were carried out assuming equality of the pressures from the virial and compressibility routes. However, the results are qualitatively similar.

The isochores calculated by us possess minima in the range of densities $0.12\simeq\rho_f^*\simeq0.19$. This range is wider than that evaluated by de Oliveira *et al.*,[11] who found that density anomalies appear for $0.12\simeq\rho_f^*\simeq0.14$.

We have also verified the results of our calculations by comparing the structural order parameter s_2^* [see Eq. (7)] evaluated using the pair correlation function resulting from the HNC closure with the results reported in Fig. 4 of the recent work of Krekelberg *et al.*[15]

Figure 1(a) shows the dependencies of the fluid density on the chemical potential at two relatively high temperatures, $T_f^*=1.0$ and 0.5, as well as at low temperature, $T_f^*=0.1$. Simulation data are displayed as symbols, and the HNC results are given by lines. The HNC results for the chemical potential were obtained from the expression explored in several works, see e.g., Ref. 20,

$$\beta\mu=-\rho_f\int d\mathbf{r}c_{ff}(r)+\frac{1}{2}\rho_f\int d\mathbf{r}h_{ff}(r)(h_{ff}(r)-c_{ff}(r)). \tag{11}$$

At high values of the chemical potential all the isotherms are almost linear and the differences between them become smaller and smaller when the chemical potential increases. This serves as manifestation of negligible effects of attractive interaction and of the soft ramp repulsion in comparison to the predominant effect of the repulsive core of the Lennard-Jones potential. At lower chemical potential values the curves ρ_f^* versus μ^* are nonlinear. The nonlinearity is only marginal at higher temperatures, but increases with temperature decrease and at $T_f^*=0.1$ the isotherm is strongly nonlin-

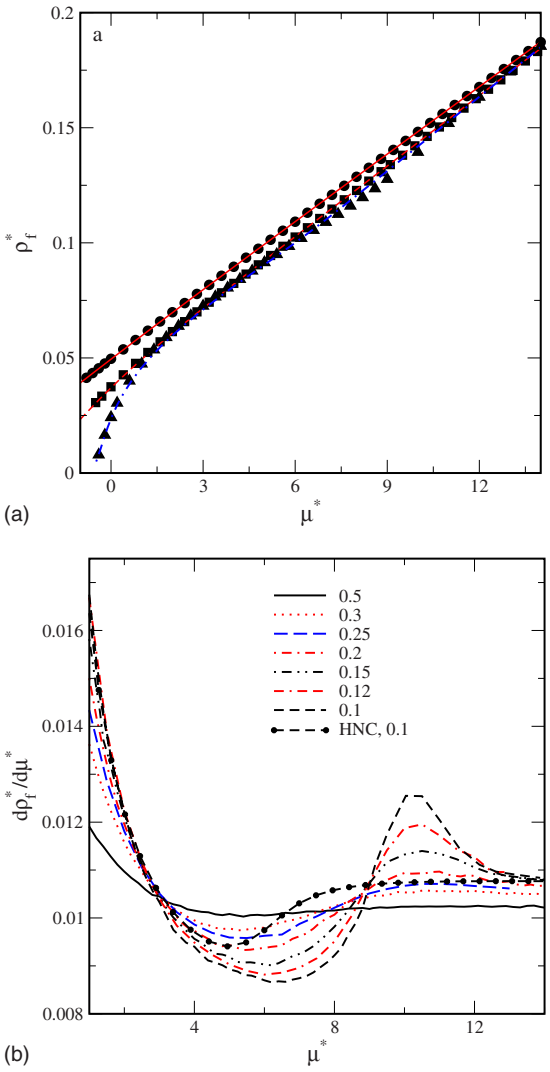

FIG. 1. (Color online) (a) Equation of state in terms of the dependence of fluid density on the chemical potential. The GCMC data are given as symbols whereas the lines come from the HNC closure. Circles and solid line are for $T_f^*=1.0$, squares and the short-dashed line are for $T_f^*=0.5$ whereas triangles and dashed-dotted line are for $T_f^*=0.1$, respectively. (b) The derivative $d\rho_f^*/d\mu^*$ from simulations (the nomenclature of lines is given in the figure) and from the HNC approximation at lowest temperature considered, $T_f^*=0.1$.

ear at low values of the chemical potential. However, we have observed that the isotherms change inclination at low temperatures. Thus, it is of interest to explore the behavior of $d\rho_f^*/d\mu^*$ in more detail.

We have found that in the case of simulation data the derivative $d\rho_f^*/d\mu^*$ is high at low μ^*, next it decreases with an increase of μ^* and then grows again [Fig. 1(b)]. For the moment, we just call the region of density between the minimum and maximum of the derivative as the region of anomaly coming from isotherms and will return to the analysis of the limits of this region below, after obtaining other properties, particularly the order parameters given by Eqs. (7) and (8).

It is worth to comment that the overall agreement between the ρ_f^* versus μ^* isotherms evaluated from the HNC approximation and simulations is quite reasonable. However, larger disagreement can be seen at low temperature, especially within the density region, where the density anomaly has been reported.[10,11] In order to get a more profound insight into the performance of the HNC approximation, in Fig. 2 we present a comparison of GCMC and HNC data for the changes of the chemical potential on temperature along different isochores. For $\rho_f^*=0.09$ and $\rho_f^*=0.175$ (both these values are outside of the density anomaly region according to Refs. 10 and 11) computer simulations predict that the chemical potential grows with decreasing temperature, reaches a maximum around $T_f^*\simeq 0.25$ and then decreases with decreasing temperature. Inside the region of density anomaly, e.g., for $\rho_f^*=0.127$, the chemical potential monotonously grows with decreasing temperature. For two densities outside the anomaly region the HNC results agree qualitatively with simulations. In contrast, at $\rho_f^*=0.127$ the HNC fails to follow simulation data qualitatively.

On the basis of the GCMC data we can make a rough estimate for the anomalous behavior region of the μ^* versus T_f^* dependence (in which the curves lack maximum) yielding $0.125\simeq\rho_f^*\simeq 0.140$. Actually, there exist some imprecision in these data, because the chemical potential is the control variable in simulations from which the fluid density results. Moreover, one needs to perform simulations of many isotherms at different low temperatures using fine temperature resolution. We have been satisfied to establish estimate for this interval using chemical potential variable and observe approximate coincidence with the density anomaly region evaluated from the canonical ensemble MD simulations.[11]

The microscopic structure and its evolution in the space of external parameters determine thermodynamics and influences dynamic properties of the model as well. Perfect agreement between theory and simulation at the level of microscopic structure would guarantee an accurate prediction of thermodynamic properties. In four panels of Fig. 3 we show the pair distribution functions (pdfs) coming from GCMC simulations (symbols), from the HNC approximation (solid lines) and the RY self-consistent closure (dashed lines). All these data were obtained at an intermediate temperature, $T_f^*=0.2$. The simulations predict growth of the principal maximum of the pdf at $r^*\simeq 2.0$, if the fluid density increases up to a certain value. Next, with further increase in the density, the maximum begins to decrease in expense to the appearance and growth of the maximum at smaller interparticle separation, $r^*\simeq 1.0$. These trends result in changes in the average number of particles in the coordination shells around a chosen particle.

Similar behavior was emphasized recently in Ref. 15 at the same and slightly higher temperatures for the data coming from MD simulations and the HNC closure. We would like to stress that the RY approximation describes the principal maximum of the pdf very well until the density reaches the value $\rho_f^*\simeq 0.10$. Moreover, it predicts well initial stage of the development of an additional maximum at a smaller interparticle distance, cf. Figs. 3(a) and 3(b). In the investigated range of densities, the HNC results are worse comparing to the RY data. The HNC approximation overestimates the height of the maximum at small separation and underestimates the height of the principal and the following maxima of the pdf. In contrast, at high fluid densities [Figs. 3(c) and

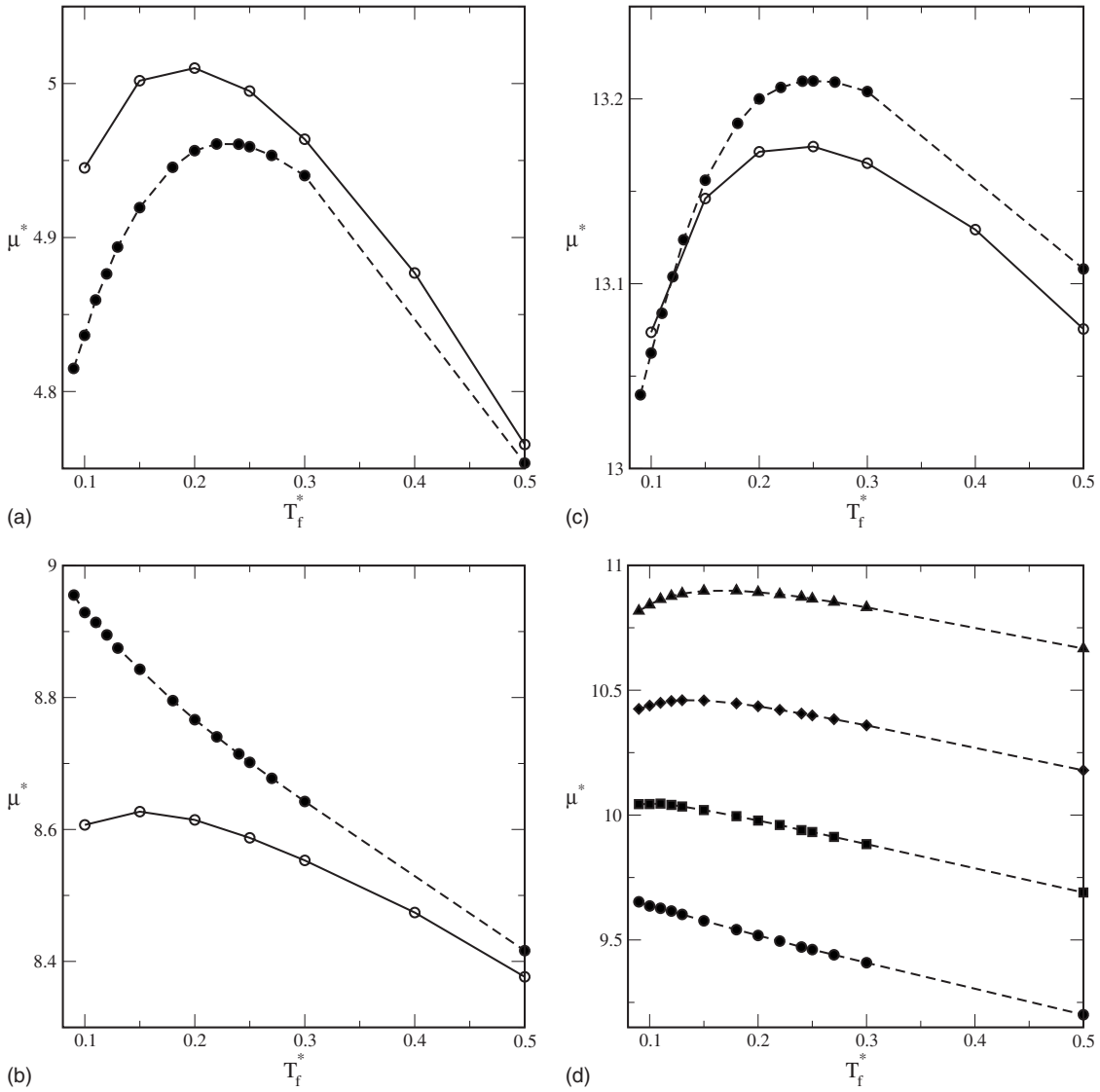

FIG. 2. Temperature dependence of the chemical potential for the bulk core-softened model fluid at constant fluid density. The GCMC data are filled symbols joined by short-dashed lines for better visualization. The HNC results are shown as solid lines with empty symbols. (a), (b), and (c) are for the fluid density $\rho_f^*=0.09$, 0.127, and 0.175, respectively. (d) contains the GCMC data solely. The circles, squares, diamonds, and triangles are for the fluid density $\rho_f^*=0.135$, 0.14, 0.145, and 0.15, respectively.

3(d)], the HNC closure performs better in comparison to more sophisticated RY approximation. In particular, at the highest density studied here, $\rho_f^*=0.20$, the HNC reproduces the heights and the positions of all the maxima of the pdf. Small discrepancies between GCMC data and HNC results are observed for the first pdf maximum, if the density is close to the upper limit of the density anomaly range, $\rho_f^* \simeq 0.14$.

More demanding tests of the pdfs are given in Fig. 4. The calculations were carried out at lower temperature, $T_f^*=0.15$. In this case we observe that the RY closure reproduces reasonably well the microscopic structure at the density inside the region of anomaly, $\rho_f^*=0.125$, while the HNC result is much worse [cf. Fig. 4(a)]. At two higher densities the HNC approximation provides better agreement with simulation data than the RY closure [see Figs. 4(b) and 4(c)].

It would be seducing to evaluate the bridge function from a wide set of simulation data and then parametrize it in order to develop a more sound approximation for the microscopic structure. This issue, however, would require further efforts, together with the application of more sophisticated and thermodynamically self-consistent closures for the OZ equation, possibly at the level of the second-order OZ integral equation. From above presented results we see that neither RY nor HNC are perfect in predicting the microscopic structure of the system.

Nevertheless, we next calculated the structural order parameter s_2^*, [cf. Eq. (7)] that describes the pair correlation contribution to the fluid excess entropy[15,18] from two theoretical approaches involved, HNC and RY [Fig. 5(a)]. The s_2^* changes can be also obtained from the simulation data, see e.g., Ref. 15. We performed calculations by using the pair distribution functions from our GCMC simulation [Fig. 5(a)]. The weak and strong features of approximate theories can be seen explicitly.

The relevant plots are shown for different temperatures in Fig. 5(a). At low densities the results coming from the HNC and RY approximations flow together and do not devi-

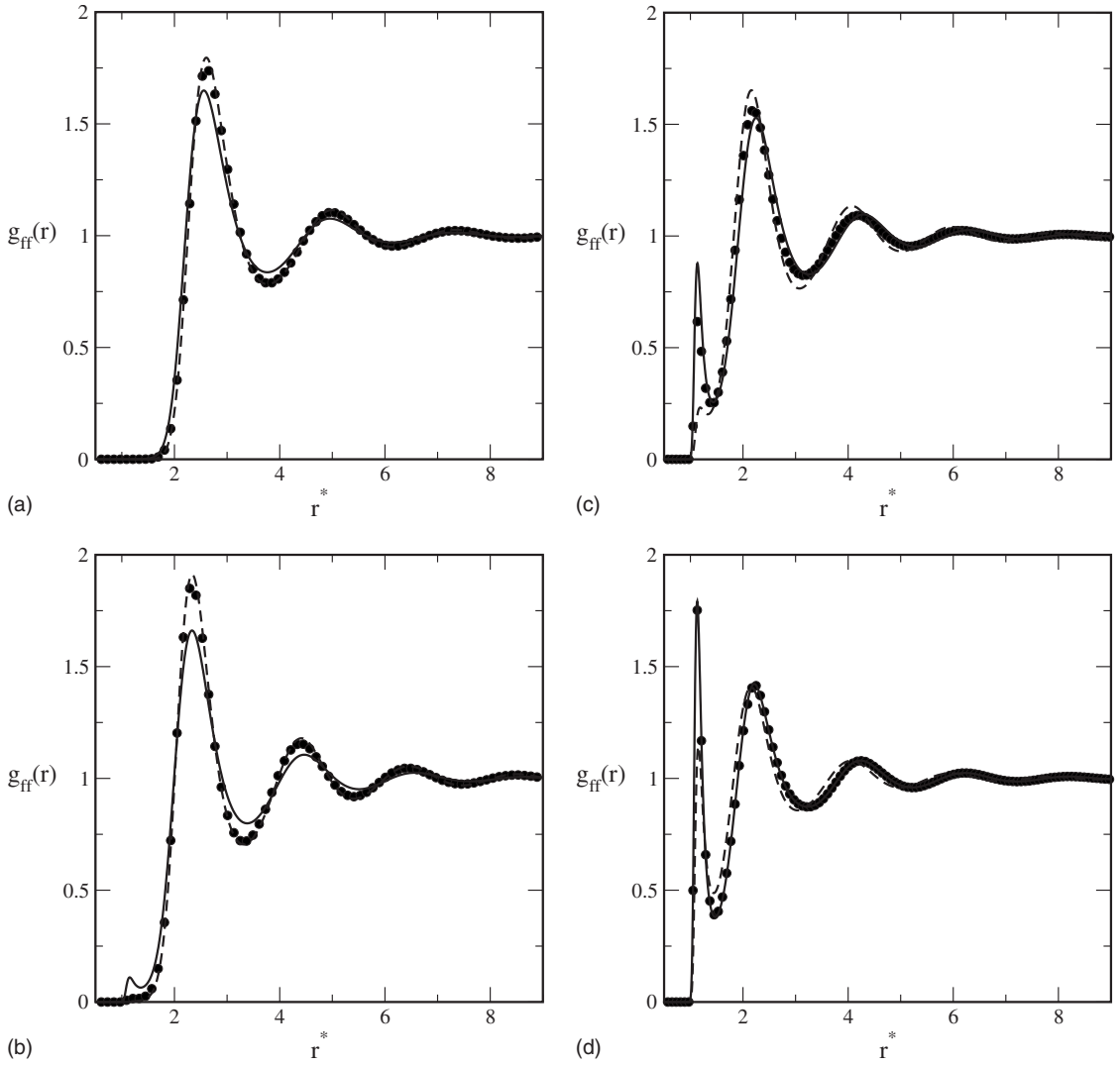

FIG. 3. A comparison of the GCMC results for the pair distribution function (filled circles) with theoretical predictions from the HNC (solid lines) and RY (dashed lines) approximations at $T_f^*=0.2$. (a), (b), (c), and (d) correspond to the following values of the chemical potential (approximate fluid density is given in parenthesis) $\mu^*=2.0(\rho_f^*=0.06)$, $\mu^*=5.5(\rho_f^*=0.095)$, $\mu^*=10.0(\rho_f^*=0.14)$, and $\mu^*=15.5(\rho_f^*=0.20)$, respectively.

ate much from computer simulation data. At high densities, e.g., $\rho_f^* \simeq 0.20$, both approximations involved predict qualitatively similar behavior, but it can be seen that the HNC performs better, in particular at low temperatures. However, the deficiency of the HNC is manifested at intermediate densities. Here, the RY results better reproduce trends observed from analysis of computer simulation data. The region of densities corresponding to the ρ_f—anomaly in which

$$\left(\frac{\partial[-s_2^*]}{\partial\rho_f^*}\right)_{T_f^*} < 0 \tag{12}$$

is at each temperature narrower for the HNC approximation than for the RY closure. Actually, the HNC underestimates the width of the region of anomalous behavior whereas the RY closure overestimates it. Moreover, the amplitude of s_2^* changes within this region is much smaller when the HNC approximation is involved.

The GCMC pdfs can be used to obtain the translational order parameter t, given by Eq. (8), Fig. 5(b). Our results agree with previously reported data of MD approach.[10] In addition, we performed calculations at lower temperatures and observed that the amplitude of variation of the order parameter increases, whereas the width of the region of anomaly slightly decreases when the fluid temperature decreases.

Now, we would like to summarize our observation concerning the location and width of the region of anomalies in thermodynamic plane. Such an insight is provided in Fig. 5(c). The circles and dashed line joining them show the borders of density anomaly region coming from the behavior of the derivative $d\rho_f^*/d\mu^*$, cf. Fig. 1(b). The squares describe limits of the region of anomaly according to the extrema of the translational order parameter, t. Finally, the stars follow from the data shown for s_2^* changes with density in Fig. 5(a). The width of anomalous region is very similar from all three criteria at low temperatures around $T_f^* \simeq 0.1$. At high temperatures the lower border of the anomalous region is also quite similar if one involves different sets of results, whereas the upper border extends to higher densities if one applies criterion of translational order parameter t, comparing to other criteria, $d\rho_f^*/d\mu^*$ and s_2^*. The observed picture closely

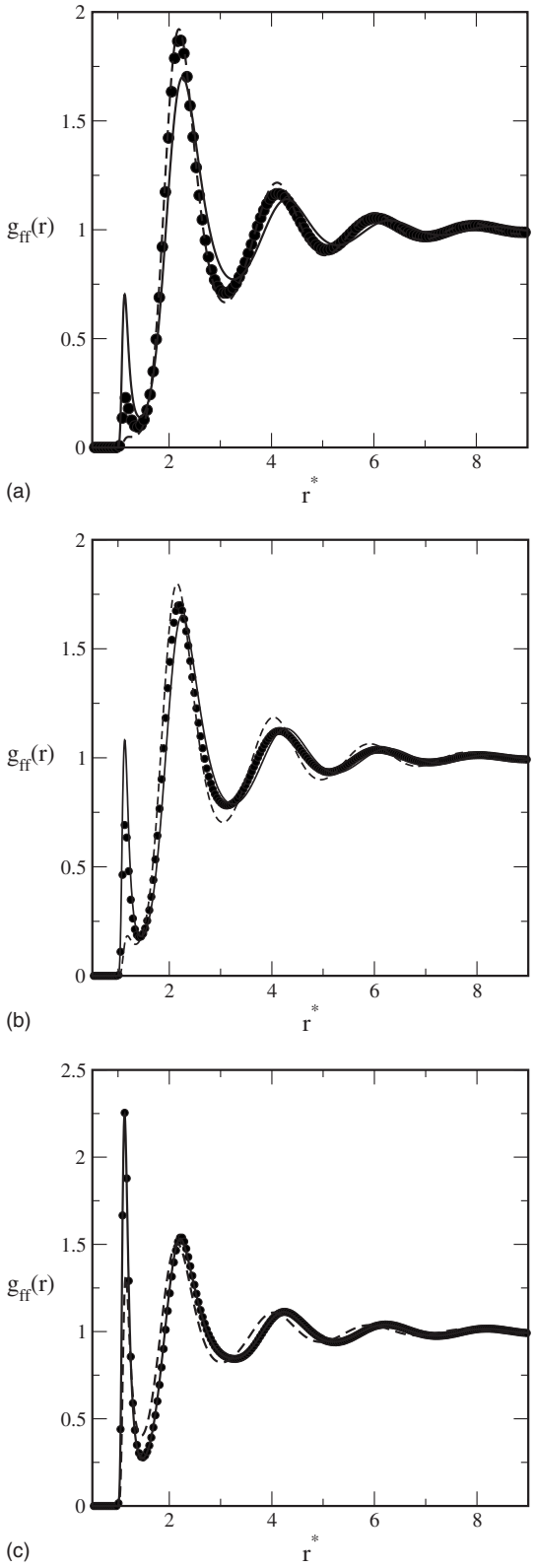

FIG. 4. The same as in Fig. 3 but at $T_f^*=0.15$. (a), (b), and (c) correspond to the following values of the chemical potential (approximate fluid density is given in parenthesis) $\mu^*=8.6(\rho_f^*=0.125)$, $\mu^*=10.0(\rho_f^*=0.14)$, and $\mu^*=15.5(\rho_f^*=0.20)$, respectively.

resembles what has been discussed using MD data but involves our own GCMC simulations and results for the chemical potential.

Now, we are able to establish a certain link of the present

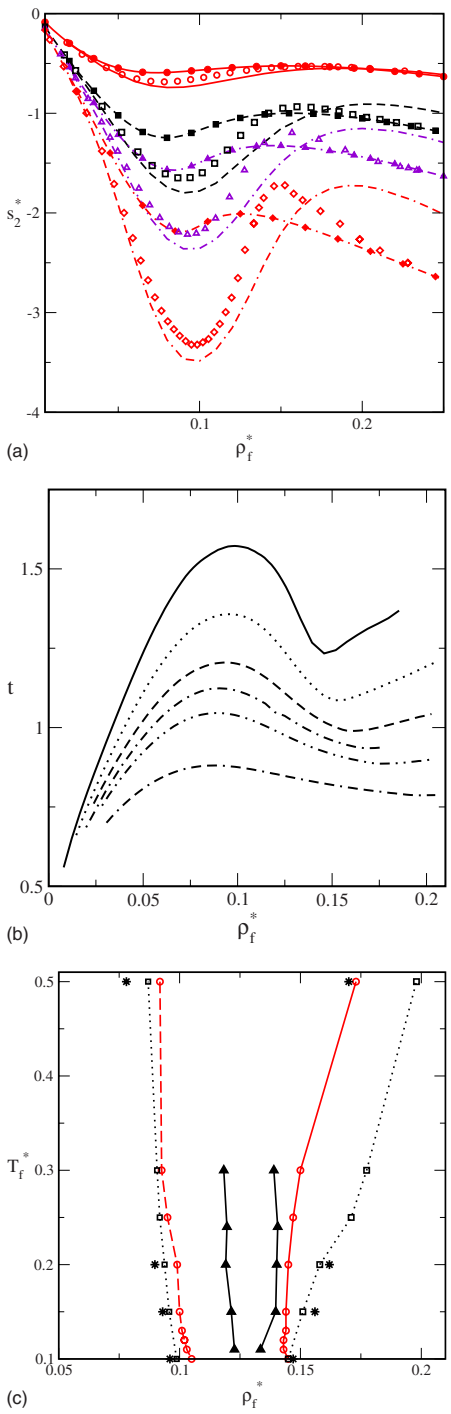

FIG. 5. (Color online) (a) The density dependence of the reduced pair excess entropy from the RY (lines) and HNC (the same type of lines marked with symbols) approximations at $T_f^*=0.5$ (solid lines and circles), $T_f^*=0.2$ (short-dashed lines and squares), $T_f^*=0.15$ (dashed-dotted lines and triangles) and $T_f^*=0.1$ (double dashed-dotted lines and rhombs), respectively. Solely empty symbols show the results obtained by integrating the distribution functions from GCMC simulation for each temperature in question. (b) The dependence of the value for translational order parameter on fluid density from computer simulated distribution functions. The solid, dotted, dashed, dotted-dashed, double dotted–dashed, and double dashed–dotted lines are for $T_f^*=0.1$, $T_f^*=0.15$, $T_f^*=0.2$, $T_f^*=0.25$, $T_f^*=0.3$, and $T_f^*=0.5$, respectively. (c) The region of anomalous behavior in the temperature-density plane from computer simulations. Circles result from extrema of the derivative $d\rho_f^*/d\mu^*$, cf. Fig. 1(b), squares are plotted by using extrema of the order parameter, t, cf. (b) of this figure, stars correspond to extrema of the s_2^* values, cf. (a) of this figure and finally triangles show the region inside which the density derivative of the heat capacity is negative. Lines are given to guide an eye.

observations and the results for the dependence of chemical potential on temperature at different fluid densities, cf. Fig. 2. Namely, we see that if the density is inside the anomalous region the $\mu^*(T_f^*)$ does not show maximum. In contrast, the presence of maxima on this dependence signalizes that the fluid density crosses either the lower border of anomalous region or its upper border. In fact, we can apply the chain relation to obtain

$$(d\mu^*/dT_f^*)_{\rho_f^*} = (d\mu^*/d\rho_f^*)_{T_f^*}(d\rho_f^*/dT_f^*)_{\mu^*}. \quad (13)$$

The left hand side is zero for the set of densities delimiting the anomaly region, cf. Fig. 2 and is nonzero for the densities inside the anomaly region. Also, we have observed that the derivative $(d\rho_f^*/d\mu^*)_{T_f^*}$ has extrema but is nonzero for the entire range of temperatures studied, cf. Fig. 1(b). Thus, the zero values of the left hand side of the above equation really can be attributed to the borders of anomalous region because the derivative $(d\rho_f^*/dT_f^*)_{\mu^*}$ has the same meaning and is closely related to $(d\rho_f^*/dT_f^*)_P$. However, to use such criteria for establishing borders of anomalous region requires a big amount of simulation data.

Our previous considerations have been concerned with simulation data and theoretical results that involve solely integration of the pair distribution functions at a given thermodynamic state. One of the most stringent tests of the accuracy of integral equation results is provided if one attempts the calculation of heat capacity. In the course of the GCMC simulation we have calculated the fluctuations of the Hamiltonian of the system, cf. Eq. (5). On the other hand, reduced heat capacity can be obtained in the framework of theoretical approaches according to Eq. (9). This expression involves temperature derivative of the correlation functions, however.

Heat capacities (normalized by the volume, $\overline{c_V}\rho_f^*$, from simulations and two theories involved are given in Fig. 6. We observe that the heat capacity begins to exhibit peculiar behavior in the region of temperatures below $T_f^* \simeq 0.20$ [Fig. 6(a)]. There is a qualitative agreement between two theories and simulation only at high temperature, e.g., $T_f^*=0.5$. For all lower temperatures the theories follow computer simulation results only at low densities. Both theoretical approaches fail to describe the heat capacity. However, inspecting such a disappointing picture one can claim that the RY closure is slightly better comparing to the HNC approximation at intermediate densities. These trends are in agreement with our observations concerning the behavior of $s_2^*(\rho_f^*)$ from the HNC and RY closures in the anomaly region. The discrepancy of theoretical results with respect to simulation data can be intuitively explained as follows. The HNC approach is not thermodynamically self-consistent. On the other hand, the RY approach reaches consistency through fitting the virial and compressibility pressures. If one would require stronger consistency involving energy route to thermodynamics, then better results for the properties determined by temperature derivatives should be reached. This issue must be explored in more detail. Nevertheless, computer simulations clearly show that the region where $dc_V^*/d\rho_f^*$ is negative is much narrower than the anomalous regions coming from other criteria both at low and at high temperatures, cf. Fig. 5(c).

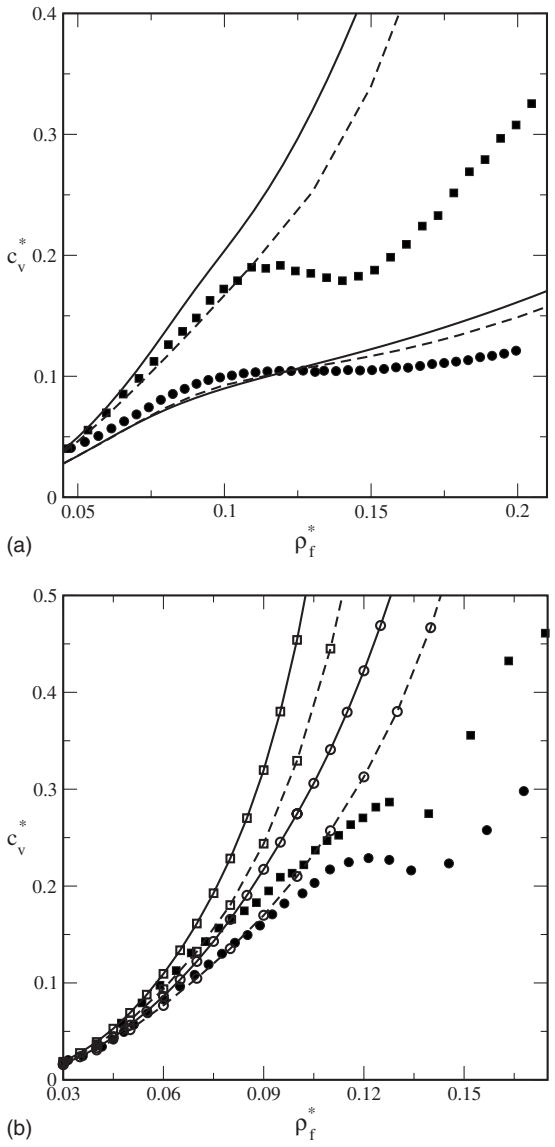

FIG. 6. The dependence of the reduced heat capacity (normalized by volume) on fluid density from the GCMC simulation (symbols) and HNC (solid lines) and RY (dashed lines) approximations. (a) $T_f^*=0.5$—circles $T_f^*=0.2$—squares. (b) $T_f^*=0.15$—circles and $T_f^*=0.1$—squares. In part b the lines are marked by empty symbols to visualize correspondence to the GCMC data better.

Due to negligible effects of attractive interaction in the model with the chosen set of parameters, the liquid-vapor transition does not occur.[21,22] However, when the density increases and/or the temperature decreases, the fluid can transform either into a glass or a solid. A rough estimate of the conditions leading to such phases can be obtained by inspecting the behavior of the structure factor. Namely, according to the empirical Hansen–Verlet criterion, a liquid crystallizes when the structure factor at its highest maximum attains the quasi-universal value 2.85. It is worth mentioning that this criterion has been deduced from the behavior of the fluid of hard spheres. The behavior of the structure factor at high fluid densities has been investigated recently for a Gaussian core model.[23] However, a Gaussian core potential is bounded in contrast to the unbounded interaction of this study given by Eq. (1). The Gaussian model, in spite of absence of a hard

core, shares some similarity with the model in question due to slowly decaying repulsion that extends to quite large distances between particles. Interestingly, the Gaussian core model is characterized by a set of anomalies (elucidated by Monte Carlo simulations).[24] On the other hand, it is known that the models with bounded interactions are characterized by peculiarities in the region of high densities. Namely, the clustering transition and re-entrant melting have been observed.[25,26]

Let us proceed now to the description of the behavior of the structure factor. Having confidence in the quality of the HNC approximation at high densities [cf. Figs. 3(d), 4(c), and 5(a)], we apply this closure to evaluate the structure factor. The relevant results are given in Figs. 7 and 8. At an "intermediate" temperature, $T_f^*=0.2$, the structure factor is characterized by growing first maximum and developing oscillations if the density grows from $\rho_f^*=0.05$ to $\rho_f^*\simeq 0.20$, see Fig. 7(a). Next [Fig. 7(a)], the height of the first maximum at $Q\simeq 3.2$ saturates, and then it starts to decrease with further increase of fluid density. The amplitude of oscillations at higher wavevectors increases with density in the entire range of densities shown in this figure. The second maximum is located at $Q\simeq 6.5$. Further increase of density [Fig. 7(b)] results in decreasing the first maximum, whereas the second maximum shifts slightly, it is located at $Q\simeq 6.75$ at a highest density studied. The second maximum strongly grows up and overcomes the value of 2.85 at $\rho_f^*\simeq 0.76$, see Fig. 7(b). The distance between subsequent maxima on the structure factor is $Q\simeq 5$. The pdfs describing the evolution of the structure at high densities and growth of the number of nearest neighbors are shown in Fig. 7(c). We observe that when the height of the first peak of the structure factor overcomes 2.85, the corresponding microscopic structure in terms of the $g_{ff}(r)$ is characterized by a very high first maximum and well-pronounced maxima for the second, third, fourth, and even fifth coordination shells. All these maxima are separated by a distance approximately equal to σ_f.

The trends observed for a lower temperature, bear some similarity to discussed above but exhibits certain important differences, cf. Figs. 8(a)–8(d) for the case $T_f^*=0.1$. In the region of low densities the first maximum of the structure factor at $Q\simeq 3.2$ again saturates, but its height becomes higher than the value 2.85 at the density around $\rho_f^*\simeq 0.20$, Fig. 8(a). The second maximum is well developed and is separated by the distance $Q\simeq 3$ from the first one. The distance between the second and much less developed third maximum of the structure factor is of the order $Q\simeq 6$ at a highest density in this panel, $\rho_f^*\simeq 0.20$. The corresponding changes in the structure in r-space are shown in Fig. 8(b). The first and second peaks of the pdf are quite high. One can argue that such behavior resembles the formation of a small "cluster" of particles. There is no maximum at $r\simeq 3$ in contrast to our observation of the structure in Fig. 7(c). However, due to the oscillations of the structure factor, i.e., from the existence of the second and third maxima at these conditions, we can argue that there exist some trends to ordering of these clusters at large-distance scale.

At still higher densities, Fig. 8(c), the behavior of the structure factor is similar to that in the discussion of Fig. 7(b). In the region of higher densities the first peak of the structure factor decreases after saturation, whereas the second peak grows and overcomes the quasiuniversal value of the Hansen–Verlet criterion 2.85 at $\rho_f^*\simeq 0.62$. As at a higher temperature, $T_f^*=0.2$, this second maximum is located at Q

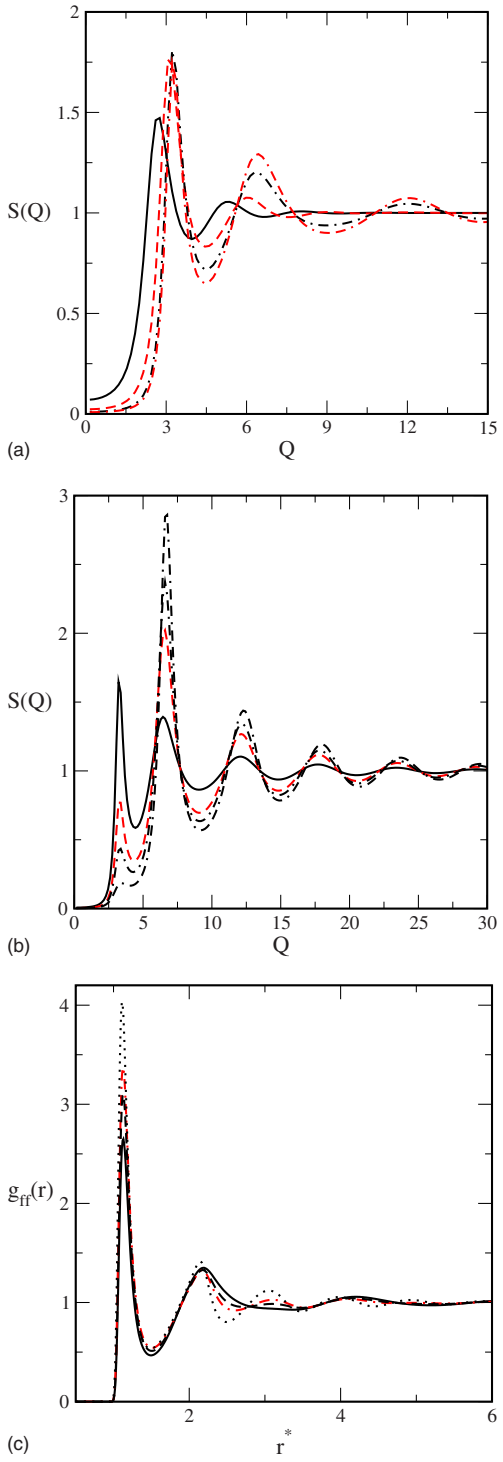

FIG. 7. (Color online) The density dependence of the structure factor [panels (a) and (b)] and pdf [panel (c)] from the HNC approximations at $T_f^*=0.2$. (a) The solid, short-dashed, dashed-dotted, and double dashed–dotted lines are for the fluid density $\rho_f^*=0.05$, 0.10, 0.20, and 0.25, respectively. (b) The solid, short-dashed, dashed-dotted, and double dashed–dotted lines are for the fluid density $\rho_f^*=0.30$, 0.55, 0.65, and 0.76, respectively. (c) $g_{ff}(r)$ for $\rho_f^*=0.30$ (solid line), 0.40 (dashed line), 0.50 (dashed-dotted line), and 0.76 (dots), respectively.

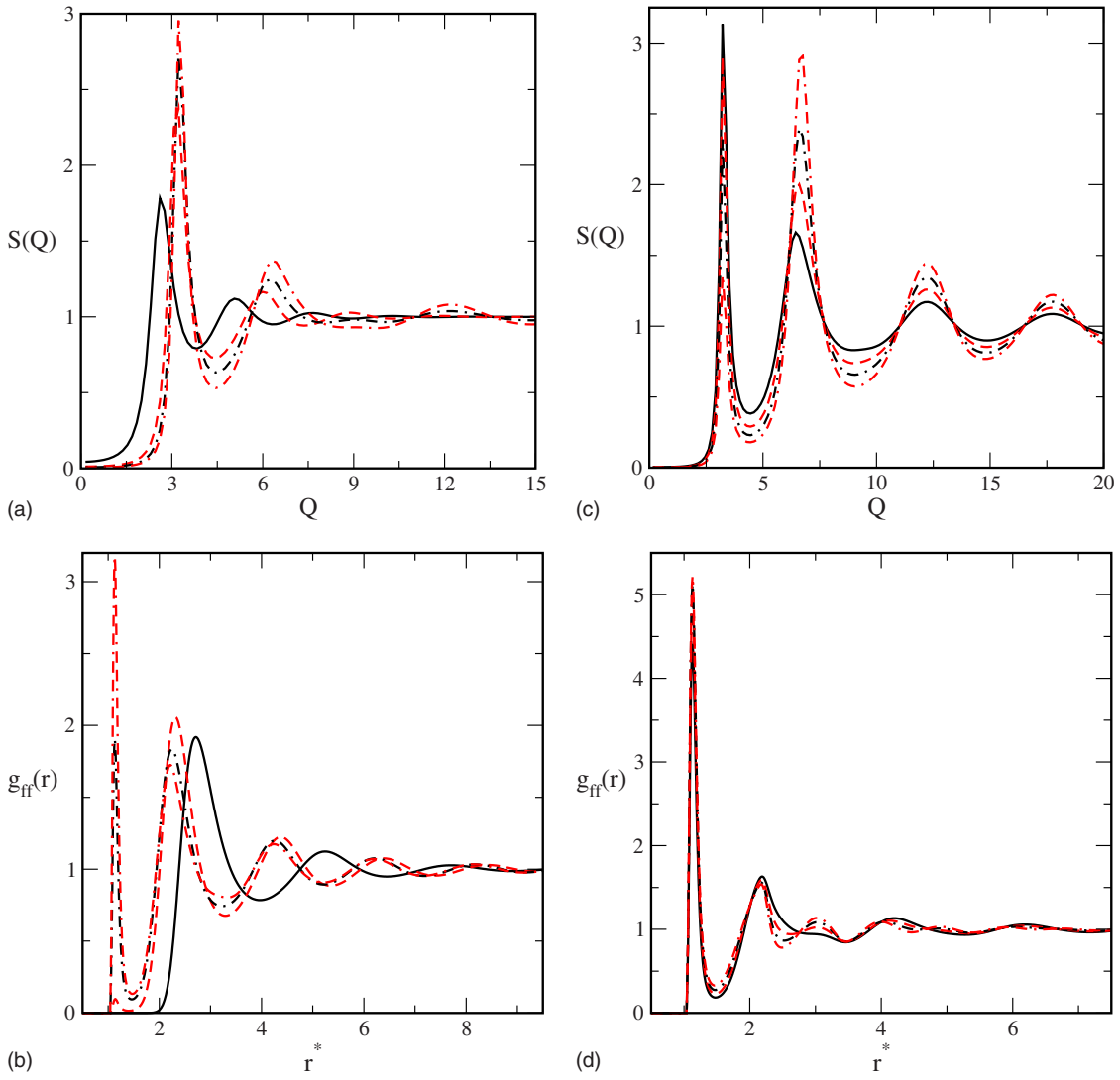

FIG. 8. (Color online) The same as in Fig. 7, but at $T_f^*=0.1$. (a) The solid, short-dashed, dashed-dotted, and double dashed–dotted lines are for the fluid density $\rho_f^*=0.05$, 0.10, 0.15, and 0.20, respectively. (b) $g_{ff}(r)$ for the same densities as in part a (the nomenclature of lines as in part a). (c) The solid, short-dashed, dashed-dotted, and double dashed–dotted lines are for the fluid density $\rho_f^*=0.30$, 0.40, 0.50, and 0.62, respectively. (d) $g_{ff}(r)$ for the same densities as in (c) [the nomenclature of lines as in part (c)].

$\simeq 6.75$. Again, the distance between the second and well-pronounced subsequent maxima (third, fourth, etc.) approximately is $Q \simeq 5$. The corresponding structure in the r-space is shown in Fig. 8(d). It closely resembles the structure in Fig. 7(c), i.e., the presence of at least five coordination shells separated by approximately constant distance σ_f. So, the principal difference between the structures observed at a higher [Figs. 7(b) and 7(c)] and lower [Figs. 8(a)–8(d)] temperatures is that in the latter case an "intermediate" ordering of small clusters is observed prior to the formation of crystal-like order if one accepts the Hansen–Verlet criterion. Also, one must take into account not only the height of the first maximum of the structure factor but also its position while interpreting observed structures according to this criterion.

Possible crystallization and relevant structures of solid phases of the core-softened fluid should be explored in further detail by applying a wider set of available criteria similarly to Ref. 27 as well as by performing specifically focused computer simulations including analysis of the two-dimensional systems of this sort.

IV. GLASS PHASE OF THE CORE SOFTENED MODEL

In the final part of this work we would like to include theoretical analysis of the conditions at which the core-softened model in question transforms into a glass phase. This issue is of interest on its own and has not been explored so far. Moreover, theoretical developments presented below are intrinsically related to the method of integral equations and specifically to the hypernetted chain approximation described above. The approach we use here has been proposed first in Refs. 28 and 29 and applied to study glass phase formation in the fluid of hard spheres. Only the final ingredients of the theory are given below, the reader is referred to original publications[28,29] for a comprehensive explanation.

The principal idea is to explore the configurational excess entropy of the system at glass formation in terms of the effective potential. The effective potential follows from the overlap function describing relative "distance" between different configurations in the phase space.

Technical aspects of the final stage of the theory can be

resumed as follows. The principal task of the approach is to solve the replicated OZ (ROZ) integral equations,

$$h_{00}(r_{12}) - c_{00}(r_{12}) = \rho_0 \int d\mathbf{r}_3 c_{00}(r_{13}) h_{00}(r_{32}) + s\rho_1 \int d\mathbf{r}_3 c_{01}(r_{13}) h_{10}(r_{32}), \quad (14)$$

$$h_{10}(r_{12}) - c_{10}(r_{12}) = \rho_0 \int d\mathbf{r}_3 c_{10}(r_{13}) h_{00}(r_{32}) + \rho_1 \int d\mathbf{r}_3 [c_{11}(r_{13}) + (s-1)c_{12}(r_{13})] h_{10}(r_{32}), \quad (15)$$

$$h_{11}(r_{12}) - c_{11}(r_{12}) = \rho_0 \int d\mathbf{r}_3 c_{10}(r_{13}) h_{10}(r_{32}) + \rho_1 \int d\mathbf{r}_3 c_{11}(r_{13}) h_{11}(r_{32}) + (s-1)\rho_1 \int d\mathbf{r}_3 c_{12}(r_{13}) h_{12}(r_{32}), \quad (16)$$

$$h_{12}(r_{12}) - c_{12}(r_{12}) = \rho_0 \int d\mathbf{r}_3 c_{10}(r_{13}) h_{10}(r_{32}) + \rho_1 \int d\mathbf{r}_3 c_{11}(r_{13}) h_{12}(r_{32}) + \rho_1 \int d\mathbf{r}_3 c_{12}(r_{13}) h_{11}(r_{32}) + (s-2)\rho_1 \int d\mathbf{r}_3 c_{12}(r_{13}) h_{12}(r_{32}), \quad (17)$$

where $s+1$ is the number of replicas of the fluid system. The method is quite similar to the approach developed by Given and Stell[30–32] for the description of fluids in quenched matrices. The limit $s=0$ is taken before solving Eqs. (14)–(17). The ROZ equations are supplemented by the HNC closure in the form

$$1 + h_{ij}(r) = \exp[-\beta u_{ij}(r)] \exp[h_{ij}(r) - c_{ij}(r)], \quad (18)$$

where i,j take values 0,1 and 2. The subindices in the correlation functions denote that particles belong to a distinguished replica 0, or equivalent replicas 1 and 2. Moreover,

$$u_{00}(r) = u_{11}(r) = u_{ff}(r),$$

$$u_{10}(r) = u_{01}(r) = \varepsilon w(r), \quad (19)$$

where $w(r)$ is taken similar to the original developments[28,29] in the form

$$w(r) = 1, \quad r < 0.3\sigma_f,$$

$$w(r) = 0, \quad r > 0.3\sigma_f. \quad (20)$$

The energetic parameter ε/k_BT describes coupling (either attraction or repulsion dependent on the sign of ε) between the "reference" configuration of the fluid system chosen as replica with the number 0 and configurations corresponding to other replicas. The distinguished ($s=0$) and all other replicas are at the same density $\rho_0=\rho_1=\rho_f$. The overlap function is defined as follows:

$$q(\varepsilon) = 4\pi\rho_1 \int_0^\infty dr r^2 g_{10}(r) w(r). \quad (21)$$

The glassy behavior of the system is associated with nonconvexity of the effective potential $V(q)$,

$$V(q) = \int_a^q dq' \varepsilon(q'), \quad (22)$$

where the lower limit of integration, a, is a constant chosen for convenience of calculations. The nonconvexity of $V(q)$ in turn is related to the existence of multiple solutions of the function $q(\varepsilon)$ at vanishing and zero coupling $\varepsilon \to 0$. In the fluid phase $q(\varepsilon)$ is a single valued function, the effective potential $V(q)$ has minimum at $\rho_1 \int dx w(x)$ corresponding to the absence of any structure of the function $g_{10}(x)$ or in other words this function equals unity for all values of its argument. A strong coupling ε leads to the attraction of a system toward the reference configuration (the replica 0) and forces the function g_{10} to acquire certain structure. Similar trends of behavior are expected for the function g_{12}.

When the system approaches glass transition conditions, a solution of the ROZ/HNC will exist in which both functions $g_{10}(r)$ and $g_{12}(r)$ will have very pronounced structure even at zero coupling $\varepsilon=0$. This discussion actually is borrowed from Refs. 28 and 29 to make things clearer for the reader. On the other hand, we will show just now that additional insights into glass transition for the model in question (as well as for previously studied fluid of hard spheres) can be obtained besides resorting to the notion of effective potential. These additional insights follow from the application of the expression for the chemical potential of the replicated system in the ROZ/HNC approximation[33]

$$\beta\mu_1 = -\rho_0 \int d\mathbf{r} c_{00}(r) - \rho_1 \int d\mathbf{r} [c_{11}(r) - c_{12}(r)] + \frac{1}{2}\rho_0 \int d\mathbf{r} h_{10}(r)(h_{10}(r) - c_{10}(r)) + \frac{1}{2}\rho_1 \int d\mathbf{r} h_{11}(r)(h_{11}(r) - c_{11}(r)) - \frac{1}{2}\rho_1 \int d\mathbf{r} h_{12}(r)(h_{12}(r) - c_{12}(r)). \quad (23)$$

Let us proceed to the numerical results. The ROZ/HNC equation has been solved by iterations on a grid of 2^{12} points with the step $\delta r=0.005$ and by applying standard fast Fourier-transform routine. Our discussion below is concerned with two fluid temperatures, namely, $T_f^*=0.15$ and $T_f^*=0.1$ in order to establish relation between the glass transition density and densities at which the fluid possibly crys-

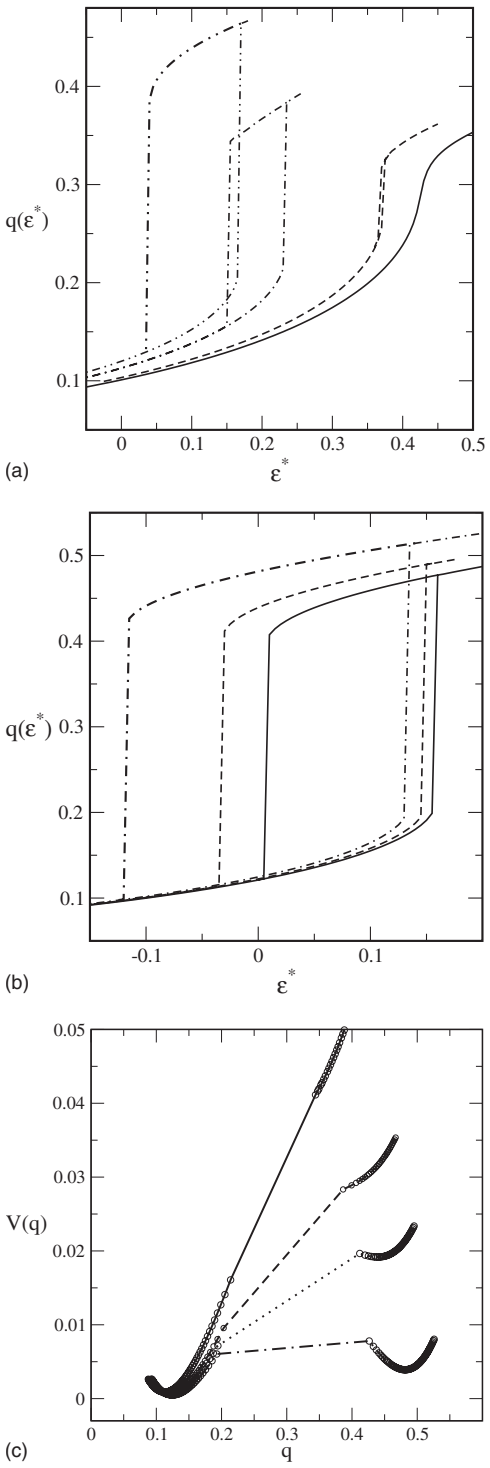

FIG. 9. [(a) and (b)] The dependence of the overlap function on the coupling parameter $q(\varepsilon^*)$ ($\varepsilon^*=\varepsilon/k_BT$) at different fluid densities along isotherm $T_f^*=0.15$. (a) The solid, short-dashed, dashed-dotted, and dashed–double dotted lines are for the fluid density $\rho_f^*=0.85$, 0.87, 0.95, and 1.01, respectively. (b) The solid, short-dashed, and dashed-dotted lines are for the fluid density $\rho_f^*=1.02$, 1.03, and 1.05, respectively. (c) The effective potential, $V(q)$, on the value of overlap. The lines and symbols from top to bottom at high q are for $\rho_f^*=0.95$, 1.01, 1.03, and 1.05, respectively.

tallizes according to Hansen–Verlet criterion. All the data presented in Figs. 9(a) and 9(b) concern with the system at reduced temperature $T_f^*=k_BT/\varepsilon_f=0.15$. We observe in Fig. 9(a) that at densities higher than $\rho_f^*\simeq 0.86$ the overlap function begins to be multivalued such that a transition between low q phase and high q phase can be induced by a coupling. In close similarity with the results previously obtained for hard sphere fluid, we identify this density as a critical density of the second-order phase transition $\rho_{cr}^*\simeq 0.86$ at which $\varepsilon_{cr}^*\simeq 0.4$. Everywhere below the normalization of the density is as common, $\rho_i^*=\rho_i\sigma_f^3$. Remember that this set refers to $T_f^*=0.15$. The line of first-order phase transitions $\varepsilon_{tr}^*(\rho_f)$ can be drawn by applying some sort of Maxwell construction, cf. Refs. 28 and 29 to several sets of data shown in Figs. 9(a) and 9(b). This line apparently terminates at $\rho_s^*\simeq 1.055$ at a slightly higher density than that shown in Fig. 9(b), $\rho_f^*\simeq 1.05$. In the case of hard sphere model analog of this density corresponds to vanishing configurational excess entropy. To clarify this issue we performed calculations of the effective potential according to Eq. (22), Fig. 9(c). Really, the effective potential begins to develop additional well-pronounced minimum at high values of overlap at density $\rho_f^*\simeq 1.025$ (i.e., when the "desorption" branch of $q(\varepsilon)$ extends to negative values of coupling ε^*), besides the minimum at small values of overlap q. The effective potential determines the glass transition density, ρ_s^*, at this temperature, $T_f^*=0.15$ equal to 1.055, when the second minimum attains zero.

From the inspection of data shown in Figs. 10(a) and 10(b) we see that the lowest density at which the chemical potentials corresponding to the branches of low and high q cross at zero coupling is slightly higher than 1.02. Our estimate for this density is $\rho_c^*\simeq 1.025$. The chemical potential at transition is well defined. In the density range $0.86<\rho_f^*\simeq 1.025$ two branches of the chemical potentials do not cross, they just show some sort of hysteresis similar to the data set presented in Fig. 9(b). The established density $\rho_c^*\simeq 1.025$ corresponds to the development of a second minimum of the effective potential in the language used in Refs. 28 and 29. The chemical potential criterion is perfectly suited to capture this density without calculation of the effective potential. The crossing of branches of the chemical potential means that the transition between phases of low and high overlap q at zero coupling, ε^*, is the equilibrium phase transition, according to this theory. However, the effective potential must be evaluated in order to find the glass transition density ρ_s^*. Avoiding unnecessary repetition of the comprehensive discussion of dynamics of the system attributed to all aforementioned densities and couplings,[28,29] we would like just to emphasize that the calculations of the overlap function and of the chemical potential in the replica HNC formalism lead to all characteristic points straightforwardly.

Next, we have performed similar calculations for lower temperature, $T_f^*=0.1$, and obtained qualitatively similar trends to already discussed in Fig. 10. Therefore, we restrict ourselves to giving solely the characteristic points at this temperature. Those are $\rho_{cr}^*\simeq 0.775$, $\varepsilon_{cr}^*\simeq 0.43$; $\rho_s^*\simeq 0.965$, $\rho_c^*\simeq 0.94$. At a density very slightly higher than 0.94 the branches of the chemical potentials corresponding to low and high values of q begin to overlap in accordance to the development of the second minimum of the effective potential, as discussed above.

As we have mentioned above, during glass transition the function $g_{10}(r)$, as well as $g_{12}(r)$ acquire certain structure.

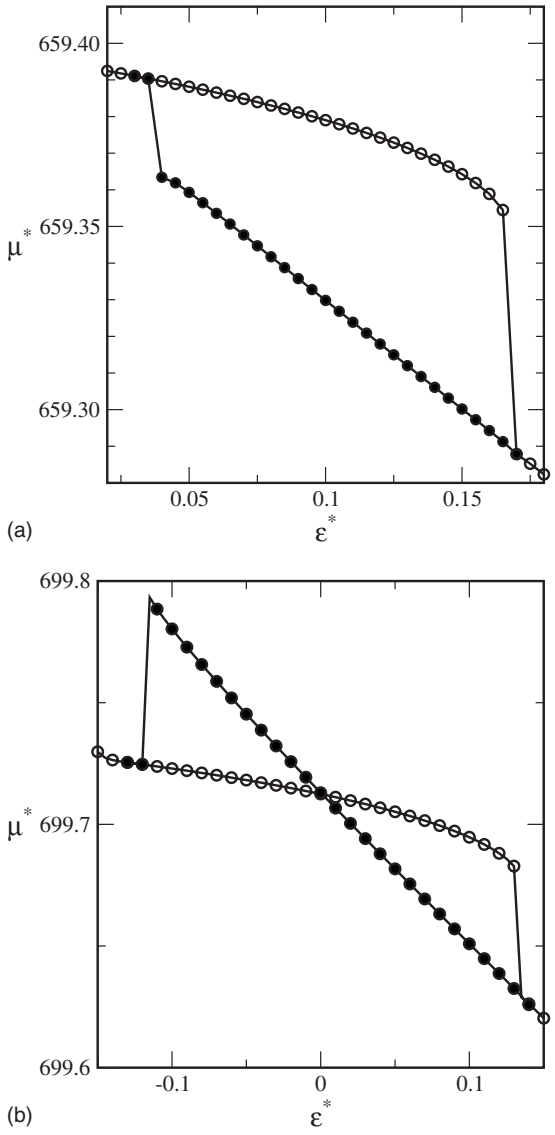

FIG. 10. The dependence of the chemical potential on the coupling parameter $\mu^*(\varepsilon^*)$ along isotherm $T_f^*=0.15$ at $\rho_f^*=1.01$ (a) and at $\rho_f^*=1.05$ (b).

One example of a change in the distribution function $g_{10}(r)$ that occurs at $\varepsilon^*=0$ at transition for $\rho_f^*=0.96$ and $T_f^*=0.1$ is shown in Fig. 11. A drastic change in the structure occurs similarly to a hard sphere model. However, in the case of a core-softened model, the maxima of $g_{10}(r)$ are not located at integer values of r^*. Moreover, a cusp at $r^*=0.3$ on this function is not visible in contrast to a hard sphere fluid undergoing glass transition. Our findings can be tested by performing computer simulations using different setup,[28,29] in comparison to standard GCMC procedure. This task is planned as a future work, however.

V. CONCLUDING REMARKS

To conclude, we have investigated the microscopic structure and thermodynamic properties of a core-softened isotropic fluid by using GCMC simulation and two integral equation theories. This model is convenient both for the Monte Carlo and molecular dynamics simulations and has received much interest recently. At this stage of the project, we have used GCMC simulations to characterize peculiari-

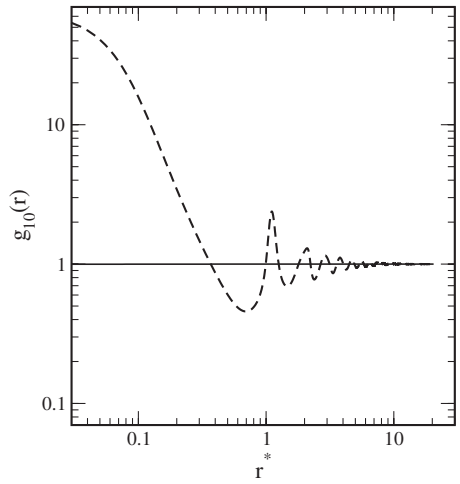

FIG. 11. The pdf $g_{10}(r)$ at $\rho_f^*=0.96$ and $T_f^*=0.1$. The solid line shows $g_{10}(r)\simeq 1.0$ on the branch of low q values at zero coupling $\varepsilon^*=0$ whereas the dashed line shows the same function at zero coupling on the branch of high q values.

ties of the dependence of density on chemical potential, in addition to properties described in previous works.[10,11,15,16] The density anomaly elucidated from previous molecular dynamics simulations is manifested here by the specific course of the curves showing the dependence of density upon the chemical potential at a fixed temperature. We have compared the range of the anomaly resulting from the dependence of the derivative $(d\rho_f^*/d\mu^*)_{T_f^*}$ upon the density, with the range coming out from the density dependencies of the translational order parameter, t, as well as from the values of the structural parameter s_2^*. The picture observed by us resembles that evaluated from MD simulations, cf. Fig. 7 of Ref. 10. Studying the dependence of the heat capacity on density we have realized that there exists an interval of densities and temperatures within which the derivative $(dc_V^*/d\rho_f^*)_{T_f^*}$ is negative. The range of densities at which this occurs falls into the anomaly range of $(d\rho_f^*/d\mu^*)_{T_f^*}$, but is much narrower. We should also stress that many of the results discussed in this work has been obtained at much lower temperatures than reported in previous studies.[10,11,15]

We have critically examined accuracy of the Rogers–Young and hypernetted chain approximations and shown that both these approximations are of limited accuracy and applicability dependent on the region of thermodynamic states studied. In particular we have observed that at densities higher than the anomaly range, the HNC approximation is quite accurate.

Inaccuracies of both approximate theories in the description of the microscopic structure within the anomaly density range result in inaccurate predictions of the structural order parameter. Moreover, both theories fail to describe accurately the heat capacity. We attribute the last failure to the fact that while the RY theory is constructed to assure the consistency of the virial and compressibility equations of state, the method of evaluation of the coefficient α entering the RY equation does not assure that the equation of state emerging from the energy route would give identical results. Consequently, one cannot guarantee that the temperature deriva-

tives of the pair distribution functions that are necessary to calculate the heat capacity, are accurate. Therefore, it would be desirable to develop a more sophisticated class of closures for these systems. It seems at the moment that either better parametrization of the bridge function (due to enforced consistency, see, e.g., Ref. 34) based on computer simulation results, or the application of the second-order OZ integral equations can represent alternatives to available developments. On the other hand, it seems possible that the associative type closures may be useful to apply for this class of models in order to describe preferential filling and saturation of either the closest and/or next coordination shells around a given molecule. Then thermodynamic properties should also be improved.

As we have already noted, at high fluid densities the hypernetted chain closure is a very valuable tool and predicts quite accurately the fluid structure. Moreover, in contrast to other closures it yields a closed formula for the chemical potential. This closure has been employed to obtain a set of results concerning possible crystallization of the system. Moreover, the HNC closure permits to predict conditions at which the fluid transforms into a glass. We have used an approach to study a possibility of glass transition that is based on the investigation of the hystereses of the chemical potential, in addition to the concepts developed previously.[28,29] Working at a given temperature, we have established a sequence of densities that describe the way the fluid approaches a glass phase. The lowest of them, ρ_{cr}^{*} is the point describing a second-order phase transition, from which a line of the first-order transition departs. At a certain higher density, ρ_{c}^{*}, the effective potential begins to develop the structure with two minima. At this density, two branches of the chemical potential begin to cross. The crossing of branches of the chemical potential means that the transition between phases of low and high overlap q at zero coupling, ε^{*}, is the equilibrium phase transition, according to this theory. At still higher density, ρ_{s}^{*}, the configurational entropy vanishes according to the behavior of the effective potential and determines glass transition point. All three densities, ρ_{cr}^{*}, ρ_{c}^{*}, and ρ_{s}^{*} depend on the temperature. It is worth mentioning that the characteristic densities evaluated in the framework of this theory are higher than those for the onset for crystallization, resulting from the Hansen–Verlet criterion. These findings are interesting on their own and for a future research in this area.

ACKNOWLEDGMENTS

This project has been partially supported by the National University of Mexico under Grant No. IN-223808-2.

[1] F. X. Prielmeier, E. W. Lang, R. J. Speedy, and H. D. Ludermann, Phys. Rev. Lett. **59**, 1128 (1987).
[2] F. Sciortino, A. Geiger and H. E. Stanley, Nature (London) **354**, 218 (1991).
[3] J. R. Errington and P. G. Debenedetti, Nature (London) **409**, 318 (2001).
[4] P. G. Debenedetti, J. Phys.: Condens. Matter **15**, R1669 (2003).
[5] C. A. Angell, R. D. Bressel, M. Hemmatti, E. J. Sare, and J. C. Tucker, Phys. Chem. Chem. Phys. **2**, 1559 (2000).
[6] M. S. Shell, P. Debenedetti, and A. Z. Panagiotopoulos, Phys. Rev. E **66**, 011202 (2002).
[7] A. Barros de Oliveira, G. Franzese, P. A. Netz, and M. C. Barbosa, J. Chem. Phys. **128**, 064901 (2008).
[8] P. H. Poole, F. Sciortino, U. Essmann, and H. E. Stanley, Phys. Rev. E **48**, 3799 (1993).
[9] P. A. Netz, F. W. Starr, H. E. Stanley, and M. C. Barbosa, J. Chem. Phys. **115**, 344 (2001).
[10] A. Barros de Oliveira, P. A. Netz, T. Colla, and M. C. Barbosa, J. Chem. Phys. **125**, 124503 (2006).
[11] A. Barros de Oliveira, P. A. Netz, T. Colla, and M. C. Barbosa, J. Chem. Phys. **124**, 084505 (2006).
[12] M. Girardi, A. L. Balladares, V. B. Henriques, and M. C. Barbosa, J. Chem. Phys. **126**, 064503 (2007).
[13] P. C. Hemmer and G. Stell, Phys. Rev. Lett. **24**, 1284 (1970).
[14] E. A. Jagla, Phys. Rev. E **58**, 1478 (1998).
[15] W. P. Krekelberg, J. Mittal, V. Ganesan, and T. M. Truskett, Phys. Rev. E **77**, 041201 (2008).
[16] H. Dominguez, O. Pizio, L. Pusztai, and S. Sokołowski, Adsorpt. Sci. Technol. **25**, 479 (2007).
[17] M. Allen and D. Tildesley, *Computer Simulation of Liquids* (Clarendon, Oxford, 1991).
[18] A. Baranyai and D. J. Evans, Phys. Rev. A **40**, 3817 (1989).
[19] G. Sarkisov and E. Lomba, J. Chem. Phys. **122**, 214504 (2005).
[20] L. Belloni, Chem. Phys. **99**, 43 (1985).
[21] G. Franzese, J. Mol. Liq. **136**, 267 (2007).
[22] S. A. Egorov, J. Chem. Phys. **128**, 174503 (2008).
[23] A. Lang, C. N. Likos, M. Watzlawek, and H. Loewen, J. Phys.: Condens. Matter **12**, 5087 (2000).
[24] P. Mausbach and H. O. May, Fluid Phase Equilib. **249**, 17 (2006).
[25] C. N. Likos, W. Watzlawek, and H. Loewen, Phys. Rev. E **58**, 3135 (1998).
[26] B. M. Mladek, D. Gottwald, G. Kahl, M. Neumann, and C. N. Likos, J. Phys. Chem. B **111**, 12799 (2007).
[27] F. Saija, S. Prestipino, and P. V. Giaquinta, J. Chem. Phys. **124**, 244504 (2006).
[28] M. Cardenas, S. Franz, and G. Parisi, J. Phys. A **31**, L163 (1998).
[29] M. Cardenas, S. Franz, and G. Parisi, J. Chem. Phys. **110**, 1726 (1999).
[30] J. A. Given and G. Stell, Physica A **209**, 495 (1994).
[31] J. A. Given and G. Stell, J. Chem. Phys. **97**, 4573 (1992).
[32] J. A. Given, J. Chem. Phys. **102**, 2934 (1995).
[33] B. Hribar, V. Vlachy, and O. Pizio, Mol. Phys. **100**, 3093 (2002).
[34] M. D. Carbajal-Tinoco, J. Chem. Phys. **128**, 184507 (2008).